Perturbation of BRD4 and p300 activity suppresses super enhancer-driven *KLF6* expression in renal carcinoma

NURUL NADIA MOHAMAD ZAMBERI[1,2], ASMAA Y. ABUHAMAD[3], SITI NUR HASANAH MOHD YUSUF[1], NUR QURRATU ATHIRAH A. RAHMAN[1], MOHAMAD AIMANUDDIN MOHTAR[1] and SAIFUL EFFENDI SYAFRUDDIN[1]

[1]Universiti Kebangsaan Malaysia Medical Molecular Biology Institute, Cheras, Kuala Lumpur 56000, Malaysia; [2]Faculty of Pharmaceutical Sciences, UCSI University, Cheras, Kuala Lumpur 56000, Malaysia; [3]Faculty of Health and Life Sciences, Management and Science University, Shah Alam, Selangor 40100, Malaysia

Received July 26, 2025; Accepted February 25, 2026

DOI: 10.3892/or.2026.9118

Abstract. Super enhancers (SEs) are involved in regulating cell identity and lineage-specific gene expression, and drive cancer-associated gene expression. The transcription factor Kruppel-like factor 6 (KLF6) promotes the growth and progression of clear cell renal cell carcinoma (ccRCC), with its high expression driven by one of the strongest SEs in ccRCC. However, the mechanisms that establish and maintain *KLF6* SE activity, particularly the roles of epigenetic regulators bromodomain-containing 4 (BRD4) and p300, remain poorly understood. This study investigated the roles of BRD4 and p300 in modulating *KLF6* SE activity. The effects of JQ1-mediated BRD4 and A-485-mediated p300 inhibition were assessed using cell viability and colony formation assays. Reverse transcription-quantitative (q)PCR and ChIP-qPCR were employed to evaluate the impact of BRD4 and p300 inhibition, as well as CRISPR-mediated deacetylation of individual constituent enhancers, on *KLF6* expression and SE activity. Chemical inhibition of BRD4 and p300 significantly reduced ccRCC cell viability and colony formation, and decreased *KLF6* expression and levels of acetylation at lysine 27 of histone H3 (H3K27ac) at *KLF6* enhancer regions SE_1, SE_2 and SE_3, suggesting decreased chromatin accessibility. On the other hand, deacetylation of SE_1 using dead Cas9 fused to histone deacetylase 3, led to *KLF6* downregulation, which was associated with decreased H3K27ac signals at this region. The present results demonstrated that BRD4 and p300 are key for maintaining *KLF6* SE activity and driving high *KLF6* expression in ccRCC. However, deacetylation of individual enhancer regions using CRISPR was insufficient to fully suppress *KLF6* transcription, emphasizing the robustness of the *KLF6* SE and its modular role in sustaining high *KLF6* expression. Overall, the present study deepens the understanding of growth-promoting KLF6 transcriptional networks in ccRCC and offers insights to support the development of diagnostic or therapeutic strategies.

Correspondence to: Dr Saiful Effendi Syafruddin, Universiti Kebangsaan Malaysia Medical Molecular Biology Institute, Jalan Yaacob Latiff, Bandar Tun Razak, Cheras, Kuala Lumpur 56000, Malaysia
E-mail: effendisy@hctm.ukm.edu.my

Key words: renal carcinoma, super enhancer, epigenetic modifier, transcription factor, Kruppel-like factor 6 (KLF6)

Introduction

Super enhancers (SEs) are large cluster of enhancers, characterized by abundant binding of transcription factors, cofactors and other regulatory proteins (1). These regions are notably enriched with acetylation at lysine 27 of histone H3 (H3K27ac), a histone modification that is typically associated with open chromatin regions and active transcription (1). SEs are key regulators that govern cell states and identity, and lineage-specific gene expression programs (2). Furthermore, SEs are implicated in tumorigenesis by activating the expression of pro-oncogenes that promote cell proliferation, metabolic reprogramming, cell survival and adaptability, immune response modulation and therapeutic resistance (3,4). Notably, cancer cells are dependent on SE-driven genes and the activity of these SEs require intact regulatory machinery. Perturbation of the components that maintain SE landscapes and activity can disrupt gene expression, highlighting SEs as a potential target for novel cancer therapy (5).

Small molecule inhibitors have been developed to target SE-associated regulatory proteins, including JQ1, which inhibits bromodomain-containing 4 (BRD4) (6). Serving as an epigenetic reader, BRD4 serves an important role in SE organization and transcriptional activation by binding acetylated lysine residues on histone proteins and recruiting other transcription factors and co-factors (7). Studies have shown that inhibition of BRD4 leads to the downregulation of oncogenic drivers and disrupts the SE landscape, which impairs cancer cell proliferation and fitness (8,9). In addition to BRD4, the histone acetyltransferase (HAT) p300 is also enriched at SEs, where it regulates chromatin opening, thereby facilitating the accessibility and recruitment of the transcriptional activation machinery (10). Given the dependency of cancer cells on

SE-driven genes, p300 inhibition may perturb the transcriptional activation of these genes, thus impairing cancer growth and progression (11). p300 inhibitors, such as A-485 and C646, not only hold potential as therapeutic agents but also serve as tools for studying chromatin remodeling and transcriptional regulation in cancer (11,12).

Originally identified as a bacterial adaptive immune system, CRISPR/Cas9 technology has evolved, with notable advancements extending its applications beyond traditional gene editing. The development of dead Cas9 (dCas9) variants has enabled the modulation of transcription processes and epigenetic modifications, allowing their application in study of both normal biological and pathophysiological processes (13). In particular, CRISPR/dCas9-mediated locus-specific chromatin remodeling is achieved by fusing the dCas9 protein with histone-modifying enzymes such as HAT and histone deacetylase (HDAC) (14). For example, downregulation of the zinc finger protein 334 (*ZNF334*) is associated with poor prognosis in colorectal cancer (CRC). Targeted acetylation of the *ZNF334* promoter using dCas9-p300 increases its expression, which impairs CRC cell proliferation, likely through enhanced transcriptional activation of this gene (15). By contrast, dCas9-HDAC3-mediated deacetylation of liver metastasis-promoting dipeptidyl peptidase 4 inhibits its expression and markedly decreases CRC cell proliferation and metastatic potential (16). Similar CRISPR-mediated histone deacetylation has been used to suppress mutant *KRAS* expression in CRC, which suppresses CRC cell proliferation (17). This highlights the value of CRISPR-mediated epigenome editing for studying epigenetic modification and gene expression regulation in cancer pathogenesis.

Clear cell renal cell carcinoma (ccRCC) is the most common subtype of renal cancer, characterized by biallelic von Hippel-Lindau tumor suppressor inactivation and accumulation of pro-oncogenic hypoxia-inducible factor 2α (18). The overall 5-year survival rate for ccRCC patients is 70-80% for localized disease, but decreases in advanced or metastatic cases to 10-20% despite available systemic therapies, including receptor tyrosine kinase inhibitors, immune checkpoint inhibitors and their combinations (19,20). This poor outcome is due to widespread genetic heterogeneity, the high aggressiveness of advanced-stage ccRCC and rapid development of therapeutic resistance (21-23). H3K27ac chromatin immunoprecipitation-sequencing (ChIP-Seq) profiling has revealed that one of the strongest SEs in ccRCC, characterized by large genomic locus size, high H3K27ac enrichment and occupancies by transcriptional co-activators and Mediator (1), is located near the *KLF6* locus. This SE region, which drives high expression of *KLF6* to support ccRCC pathogenesis, is insensitive to perturbation. Many SEs can be substantially disrupted by chemical or genetic perturbations, which can alter their landscape and activity (24). In contrast, the *KLF6* SE in ccRCC remains largely unaffected by CRISPR interference (CRISPRi)-mediated repression of its constituent enhancers, indicating its particular stability (25). The role of BRD4 and p300 in regulating this SE region and driving high expression of *KLF6* in ccRCC has not yet been fully elucidated. Therefore, the present study investigated the effects of chemical inhibition of BRD4 and p300 on ccRCC cell viability, *KLF6* expression and H3K27ac signals at several constituent enhancers within the *KLF6* SE locus. Additionally, the present study aimed to determine whether CRISPR/dCas9-mediated deacetylation of constituent enhancers could induce chromatin remodeling and downregulation of *KLF6* expression. To model ccRCC-specific dependencies, three genetically diverse ccRCC cell lines (786-M1A, OS-LM1B and UOK101) were used; these exhibit strong *KLF6* SE activity (25). These models were used to examine the regulatory roles of BRD4 and p300 within a disease-relevant epigenetic landscape. Understanding the regulation of SEs in ccRCC is key, as these elements are pivotal in driving oncogene expression and tumor progression, making them promising targets for therapeutic intervention in this aggressive cancer type.

Materials and methods

Cell lines and reagents. The 786-M1A and OS-LM1B human ccRCC cell lines were gifts from Professor Joan Massagué (Memorial Sloan Kettering Cancer Center, NY, USA). These cell lines are metastatic derivatives of 786-O and OS-RC2 cells, respectively (26). The UOK101 human ccRCC cell line was obtained from Dr Marston Linehan (National Cancer Institute, MD, USA). The cell lines were cultured in RPMI-1640 (Nacalai Tesque, Inc.) supplemented with 10% FBS (Tico Europe) and 1% penicillin-streptomycin solution. For lentiviral production, 293T cells (ATCC) were used and cultured in DMEM (Nacalai Tesque, Inc.) supplemented with 10% FBS and 1% penicillin-streptomycin solution. All cells were cultured at 37˚C in a humidified atmosphere containing 5% CO_2. Blasticidin (InvivoGen) and hygromycin (Nacalai Tesque, Inc.) were used for antibiotic selection to isolate cells that were successfully transduced with the dCas9-HDAC3 and sgRNA expression plasmid, respectively. JQ1 and A-485 were purchased from Sigma-Aldrich (Merck KGaA). The dCas9-HDAC3 (cat. no. 98591; Addgene, Inc.) (27) and the lentivirus packaging plasmids psPAX2 (cat. no. 12260) and pMD2.G (cat. no. 12259) were obtained from Addgene, Inc. All primers and single guide RNA (sgRNA) constructs (Table I) were purchased from Integrated DNA Technologies, Inc.

Cell viability assay. The ccRCC cells, 786-M1A, OS-LM1B and UOK101, were seeded at a density of 500-1,000 cells/well in a 96-well. On the following day, the cell culture medium was replaced with fresh medium containing the respective chemical inhibitors, JQ1 or A-485. For JQ1 treatment, concentrations of 1, 10, and 20 μM were tested, whereas A-485 was used at concentrations of 1 and 10 μM. Fresh medium containing an equivalent volume of DMSO was added to control wells, where DMSO served as the vehicle for chemical inhibitor dissolution. The treated cells were incubated at 37˚C for 72 h. The medium was replaced with 120 μl fresh medium containing AlamarBlue™ Reagent (Thermo Fisher Scientific, Inc.) at a 1:10 dilution. The cells were incubated for 2 h at 37˚C in a humidified atmosphere with 5% CO_2, protected from light. A total of 100 μl medium from each well was transferred to a black 96-well plate and fluorescence was measured using a Varioskan Flash microplate reader (Thermo Fisher Scientific, Inc.) at an excitation wavelength of 560 nm and an emission wavelength of 590 nm. A total of three wells containing

Table I. sgRNA and primer sequences.

Construct	Sequence (5'-3')
Tandem control (NTC)	ATCGAAGACAACACCGGAGTGTCGTCGTTGCTCCTAGTTTTAGAGCGCA GGTGTCGCCACCTGCGAAACACCGGGATACGGTGCGTCAATCTAGTTTT ACAGTCTTCTCG
iSE_1_KLF6	ATCGAAGACAACACCGAGAATCGCTGAAGAAACGCGGTTTTAGAGCGC AGGTGTCGCCACCTGCGAAACACCGTACTGCACTGAAGACTCGGAGTT TTACAGTCTTCTCG
iSE_2_KLF6	ATCGAAGACAACACCGACCAGCACAATTTGTCACCGGTTTTAGAGCGC AGGTGTCGCCACCTGCGAAACACCGTTGAAAAAAAACCTATCACAGTT TTACAGTCTTCTCG
iSE_3_KLF6	ATCGAAGACAACACCGATGTGGCTCTGAATCACCATGTTTTAGAGCGCA GGTGTCGCCACCTGCGAAACACCGAACGGTGAGTTCCCGGTACAGTTT TACAGTCTTCTCG
dCas9-HDAC3_SDM_forward	AGCGATGTGGAGATTAAATGTACAGGCAGTG
dCas9-HDAC3_SDM_reverse	CACTGCCTGTACATTTAATCTCCACATCGCT
ChIP qPCR iSE-1 forward	GAAGTTGAGTCCCGGTGAAA
ChIP qPCR iSE-1 reverse	ATACCCGTCCTGGGAAAATC
ChIP qPCR iSE-2 forward	TCTGTAGCTGCTGAGGCTGA
ChIP qPCR iSE-2 reverse	CACGGTGACAAATTGTGCTG
ChIP qPCR iSE-3 forward	CAGGGAGTGGAAGCTGATGT
ChIP qPCR iSE-3 reverse	CACGCTTGCTGATTTCAAAG

sgRNAs that are complementary to the targeted genomic loci are underlined. The NTC construct contains scrambled sgRNA sequences that do not match any genomic region. sgRNA, single guide RNA; NTC, non-targeting control; iSE, Clustered Regularly Interspaced Short Palindromic Repeats Interference-targeted super enhancer; KLF6, Kruppel-like factor 6; dCas9, dead Cas9; HDAC, histone deacetylase; SDM, site-directed mutagenesis; ChIP, chromatin immunoprecipitation; qPCR, quantitative PCR.

medium without cells were included as blank controls. Each treatment group consisted of five replicate wells. To determine the number of plated cells, baseline fluorescence measurements were taken on day 0 (24 h after initial seeding). The mean blank control readings was subtracted from those of each treatment well to eliminate background fluorescence. The fluorescence readings after 72 h incubation at 37˚C, were normalized to the day 0 values. Finally, the relative fluorescence of inhibitor-treated cells was calculated against that of the DMSO-treated control group. Images were acquired using an inverted light microscope (Nikon TS100).

Colony formation assay. The ccRCC cells, 786-M1A, OS-LM1B and UOK101, were seeded at a density of 100-500 cells/well in a 6-well plate. The following day, the medium was replaced with medium supplemented with either JQ1 or A-485 (1 and 10 μM). Control cells were maintained in medium containing DMSO. Following 7 days of treatment at 37˚C, the culture medium was aspirated and cells were rinsed twice with 1 ml 1X PBS. The PBS solution was then removed and the cells were fixed with 500 μl 1:1 mixture of 10% methanol and 10% acetic acid at room temperature for 15 min. The 6-well plates were placed on a horizontal shaker for 20 min at room temperature. Colonies, defined as visible cell clusters formed from a single cell, were stained with 500 μl 0.5% crystal violet staining solution (Sigma-Aldrich; Merck KGaA) for 30 min at room temperature. Excess stain was discarded and the wells were washed under running tap water. The plates were then air-dried in an oven until dry. Colony images were captured using the ChemiDoc MP imaging system (Bio-Rad Laboratories, Inc.).

For quantitative analysis of crystal violet staining, 600 μl of 10% acetic acid were added to each well, followed by incubation at room temperature on a shaker for 10 min to elute the bound dye. A 200-μl aliquot of the eluted solution was transferred to a clear 96-well plate and the absorbance was measured at 590 nm using the Varioskan Flash microplate reader (Thermo Fisher Scientific, Inc.). Absorbance values were normalized to the control wells and expressed as a percentage relative to the control group.

RNA extraction, cDNA synthesis and reverse transcription-quantitative PCR (RT-qPCR). Total RNA was extracted from ccRCC cells using TRIzol® reagent (Thermo Fisher Scientific, Inc.) according to the manufacturer's protocol. The yield and purity of total RNA were quantified using the NanoDrop™ 2000c Spectrophotometer (Thermo Fisher Scientific, Inc.). cDNA was synthesized from total RNA using a LunaScript RT SuperMix kit (New England BioLabs, Inc.) as follows: 25˚C for 2 min, 55˚C for 10 min and 95˚C for 1 min. RT-qPCR was performed using TaqMan chemistry with pre-designed TaqMan probes (Thermo Fisher Scientific, Inc.; cat. nos. KLF6 Hs00810569_m1, β-actin Hs01060665_g1) and Luna Universal Probe qPCR Master Mix (New England BioLabs,

Inc.). qPCR reactions were run on the 7500 Fast Real-Time System (Applied Biosystems; Thermo Fisher Scientific, Inc.) with the following cycling conditions: 95˚C for 1 min for initial denaturation, followed by 40 cycles of 95˚C for 15 s and 60˚C for 30 s. β-actin served as the reference gene for normalization and gene expression fold-changes were calculated using the $2^{-\Delta\Delta Cq}$ method (28).

Site-directed mutagenesis. Site-directed mutagenesis of the original dCas9-HDAC3 plasmid was performed using a PCR-based whole-plasmid amplification approach to substitute the stop codon TAA with AAA. Complementary forward and reverse primers were designed to anneal to the target region of the dCas9-hHDAC3 plasmid. This primer pair carries the nucleotide to be substituted, located in the middle of the primers (Table I).

PCR amplification was performed using Accuprime™ Pfx Supermix (Thermo Fisher Scientific, Inc.) on the Thermal Cycler T100 (Bio-Rad Laboratories, Inc.). The thermocycling conditions were as follows: Initial denaturation at 95˚C for 2 min, followed by 40 cycles of denaturation at 95˚C for 15 sec, annealing at 50-65˚C for 30 sec and extension at 68˚C for 15 min. During amplification, the forward and reverse primers anneal to opposite strands of the plasmid in their respective 5'-3' orientations and extend in opposite directions, resulting in amplification of the entire plasmid while incorporating the intended nucleotide substitution.

Following PCR amplification, the original and amplified plasmids were treated with *Dpn*I restriction enzyme (New England BioLabs, Inc.), which selectively digests the methylated original plasmid template, for 1 h at 37˚C. The undigested plasmids were transformed into *Escherichia coli* (New England BioLabs, Inc.) and selected on LB agar plates containing ampicillin. The plasmids were extracted from the transformed bacteria using the Monarch Plasmid Miniprep kit (New England BioLabs, Inc.) and subjected to Sanger sequencing (Apical Scientific, Inc.) to confirm the successful site-directed mutagenesis.

CRISPR sgRNA design. SE constituent regions at the *KLF6* locus were identified based on our previously published H3K27ac ChIP-seq dataset (accession number GSE115749) (25). Regions with the highest H3K27ac signal intensity and closest proximity to the *KLF6* locus were annotated as SE_1-3. The sgRNAs targeting these regions, iSE_1, iSE_2 and iSE_3, were described in our previous study using the webtool GPP sgRNA Designer (portals.broadinstitute.org/gppx/crispick/public) (25). The sgRNA sequences are listed in Table I. The dCas9-HDAC3 plasmid used for CRISPR-mediated deacetylation was obtained from Addgene, Inc (cat. no. 98591).

Bacteria transformation and plasmid extraction. Plasmids were introduced into chemically competent *E. coli* cells by adding the plasmid DNA directly to the competent cells, followed by incubation on ice for 30 min. Heat shock was then performed at 42˚C for 1 min, after which the tubes were immediately returned to ice for 5 min. Subsequently, 300 µl fresh Luria Bertani (LB; Sigma-Aldrich; Merck KGaA) medium was added to each tube and the cultures were incubated at 37˚C with shaking at 200 rpm for 1 h. The transformed cells were spread onto LB agar plates supplemented with ampicillin (1:1,000) for selection of successfully transformed cells and incubated overnight at 37˚C. Single colonies from LB + ampicillin plates were inoculated into 3 ml LB medium containing ampicillin (1:1,000) and cultured overnight at 37˚C in a shaking incubator at 200 rpm. Plasmids were extracted using the Monarch Plasmid Miniprep kit (New England BioLabs, Inc.) according to the manufacturer's protocol. The concentration and purity of the extracted plasmids were assessed using a NanoDrop 2000c Spectrophotometer (Thermo Fisher Scientific, Inc.).

Lentivirus production and transduction. Lentivirus was produced by co-transfecting 293T cells (ATCC) with second generation lentivirus packaging plasmids psPAX2 and envelope plasmid pMD2.G together with the plasmid of interest using the Attractene transfection reagent (Qiagen GmbH). The lentivirus plasmids were obtained from Addgene, Inc. Briefly, 1.3 µg psPAX2, 0.5 µg pMD2.G and 1.5 µg plasmid of interest were mixed, followed by the addition of 10 µl Attractene transfection reagent. The mixture was incubated at room temperature for 30 min and added to the 293T cells. Transfected cells were incubated 37˚C overnight, after which the media was replaced with fresh complete media. Lentivirus-containing media was collected 72 h post-transfection and filtered through a 0.45 µm Minisart NML syringe filter (Sartorius AG).

Cells at 60-70% confluency were transduced with filtered lentivirus-containing media in the presence of 8 µg/ml Polybrene (MilliporeSigma) and incubated at 37˚C overnight. Cells transduced with dCas9-HDAC3 plasmid were selected with 30 µg/ml blasticidin for approximately 5 days, while cells transduced with the sgRNA expression vector were selected with 1,000 µg/ml hygromycin for approximately 7 days. For validation of dCas9-HDAC3 expression by western blotting, non-transduced parental cells were maintained in parallel and used as a negative control. In addition, untransduced cells were included during antibiotic selection to monitor selection efficiency. Selection was considered complete once all untransduced cells had died, after which the antibiotic-containing medium was replaced with standard culture medium.

Protein extraction and western blotting. The transduced ccRCC cells were lysed on ice in 1X RIPA buffer supplemented with 1:100 protease inhibitor cocktail (Nacalai Tesque, Inc.). The protein concentration was quantified using the Pierce BCA Protein Assay kit (Thermo Fisher Scientific, Inc.) according to the manufacturer's instructions. Equal amounts of protein (50 µg per lane) were denatured in 1X Laemmli SDS sample buffer (GeneTex, Inc.) containing 8% β-mercaptoethanol and resolved via 8% SDS-PAGE. Proteins were transferred onto nitrocellulose membranes (GE Healthcare), which were blocked with 5% non-fat milk in 1x TBS containing 0.1% Tween-20 for 1 h at room temperature. The membrane was incubated with primary antibodies overnight at 4˚C. Following incubation with rabbit anti-mouse IgG-HRP (1:1,000; cat. no. P0260; Dako; Agilent Technologies, Inc.) for 1 h at room temperature, signals were detected using Pierce™ ECL substrate (Thermo Fisher Scientific, Inc.) and imaged using the ChemiDoc Go Imaging System (Bio-Rad Laboratories, Inc.). Primary

antibodies against Cas9 (1:500; cat. no. sc-517386) and β-actin (1:5,000; cat. no. sc-69879) (both Santa Cruz Biotechnology, Inc.) were used. The Cas9 antibody was used to detect the dCas9-HDAC3 fusion protein expressed in transduced cells. dCas9 is a catalytically inactive variant of Cas9 generated by introducing two point mutations in the nuclease domains (29). As dCas9 retains the Cas9 protein sequence, it is recognized by Cas9 antibodies and detected by western blotting.

ChIP. Cells were cross-linked with 10 ml 1% formaldehyde for 10 min at room temperature with gentle rotation to preserve protein-DNA interactions. The cross-linking reaction was quenched by adding 1 ml 0.125 M glycine and incubating cells for 5 min at room temperature with rotation. Cells were pelleted by centrifugation at 1,200 x g for 5 min at room temperature and washed twice with 15 ml cold 1X PBS. After the final wash, cell pellets were either snap-frozen and stored at -80˚C or used immediately for chromatin extraction. Frozen cells were thawed on ice and lysed in 2 ml lysis buffer composed of 20 mM Tris-HCl (pH 8.0), 150 mM NaCl, 2mM EDTA (pH 8.0), 0.1% SDS and 1% Triton X-100. The cell suspension was pipetted 10 times and incubated on ice for 5 min. Homogenization was performed on ice using a Dounce homogenizer. The homogenate was transferred to a 15-ml centrifuge tube for sonication. Chromatin was fragmented by sonication using a Branson Ultrasonics Sonifier at a frequency of 20 kHz (30 sec on/off for 15 cycles) while keeping samples on ice to minimize heat damage. The lysate was centrifuged at 18,000 x g for 20 min at 4˚C and the supernatant containing sheared chromatin was collected. A 10 μl aliquot of lysate was set aside as input control for downstream qPCR.

For IP, 100 μl magnetic protein A/G beads (Thermo Fisher Scientific, Inc.) were equilibrated three times with 1 ml 0.5% BSA (Sigma-Aldrich; Merck KGaA) in 1X PBS. The beads were resuspended in 500 μl 0.5% BSA and conjugated with 5 μg anti-H3K27ac (cat. no. ab4729) or control IgG antibody (cat. no. ab37415) (both Abcam) for ≥4 h at 4˚C on a rotating platform. The antibody-conjugated beads were washed three times with 0.5% BSA and incubated overnight at 4˚C with 600 μl chromatin lysate on a rotating platform. Beads were washed three times with low-salt wash buffer (50 mM HEPES, pH 7.5, 140 mM NaCl, 1% Triton) and once with high-salt wash buffer (50 mM HEPES, pH 7.5, 500 mM NaCl, 1% Triton). All washing steps were performed on a magnetic rack (Thermo Fisher Scientific, Inc.). To reverse cross-links and elute bound DNA, 100 μl elution buffer was added and samples were incubated at 65˚C with shaking at 1,000 rpm for 3 h. DNA was purified using the Monarch PCR & DNA Cleanup kit (New England BioLabs, Inc.) according to the manufacturer's protocol.

qPCR was performed by adding the purified, de-cross-linked DNA to a reaction mix containing 2X PowerUp SYBR Green Master Mix (Thermo Fisher Scientific, Inc.) and 10 μM forward and reverse ChIP-qPCR iSE_1, ChIP qPCR iSE_2 and ChIP qPCR iSE_3 primers (Table I). The reaction was performed using the 7500 Fast Real-Time System (Applied Biosystems; Thermo Fisher Scientific, Inc.) with the following conditions: 50˚C for 2 min, 95˚C for 2 min for initial denaturation, followed by 40 cycles of 95˚C for 3 sec and 60˚C for 30 sec. Enrichment of ChIP DNA was quantified using the percent input (% input) method (30).

Statistical analysis. Statistical analysis was performed using GraphPad Prism software (version 10.6.0; Dotmatics). Data are presented as the mean ± SD from three independent experiments unless otherwise specified. Statistical significance was tested using one-way ANOVA followed by Tukey's or Dunnett's post hoc test or an unpaired t-test with Welch's correction. $P<0.05$ was considered to indicate a statistically significant difference.

Results

BRD4 inhibition suppresses ccRCC cell viability. As BRD4 serves pivotal roles in regulating the SE landscape and transcription of downstream genes (8), the present study evaluated whether ccRCC cells are sensitive to BRD4 inhibition by JQ1. 786-M1A, OS-LM1B and UOK101 human ccRCC cells were treated with increasing concentrations of JQ1 before cell viability assays at 72 h post-treatment. BRD4 inhibition significantly decreased ccRCC cell viability in a dose-dependent manner compared with that of the vehicle-treated cells (Figs. 1A and S1A). The present study also investigated the effect of BRD4 inhibition on the colony formation of ccRCC cells. JQ1 treatment, even at a concentration of 1 μM, significantly suppressed the clonogenic potential of ccRCC cells (Figs. 1B and S1B). Overall, ccRCC cells were sensitive to JQ1-mediated BRD4 inhibition, highlighting the key role of BRD4 in supporting ccRCC cell viability.

Targeting p300 HAT decreases ccRCC cell fitness. The p300 HAT is involved in regulating chromatin accessibility and transcription activation (12). Furthermore, p300 binding is also enriched at the SE regions, driving the expression of pro-oncogenes that promote cancer progression (12). The present study aimed to assess the effect of targeting p300 activity on ccRCC cell viability by treating 786-M1A and OS-LM1B cells with 1 and 10 μM A-485 for 72 h. In both ccRCC cell lines, inhibition of p300 with 10 μM A-485 significantly decreased the viability compared with that of vehicle-treated controls, whereas treatment with a lower concentration of A-485 did not result in a significant decrease in cell viability (Figs. 2A and S2A). By contrast, colony formation assays revealed that p300 inhibition with 1 or 10 μM A-485 significantly impaired the clonogenic capacity of ccRCC cells, which was consistent with the overall trend observed in the cell viability assays (Figs. 2B and S2B). Overall, ccRCC cells exhibited sensitivity to A-485-mediated p300 inhibition, which resulted in a marked reduction in cell viability and colony formation. This suggested that p300 serves a role in controlling the expression of genes that promote ccRCC cell viability.

Expression of SE-driven KLF6 is dependent on BRD4 and p300 activity. KLF6 supports ccRCC cell proliferation by regulating cell networks through the transcriptional activation of platelet-derived growth factor β (*PDGFβ*), linking mTOR complex 1 (mTORC1) signaling pathway activity to lipid metabolism (25). While high expression of *KLF6* is driven by one of the largest SEs in ccRCC (25), the roles of BRD4 and p300, key regulators of SEs and transcription activity, remain underexplored. Therefore, the present study investigated whether targeting of BRD4 and p300 with their respective

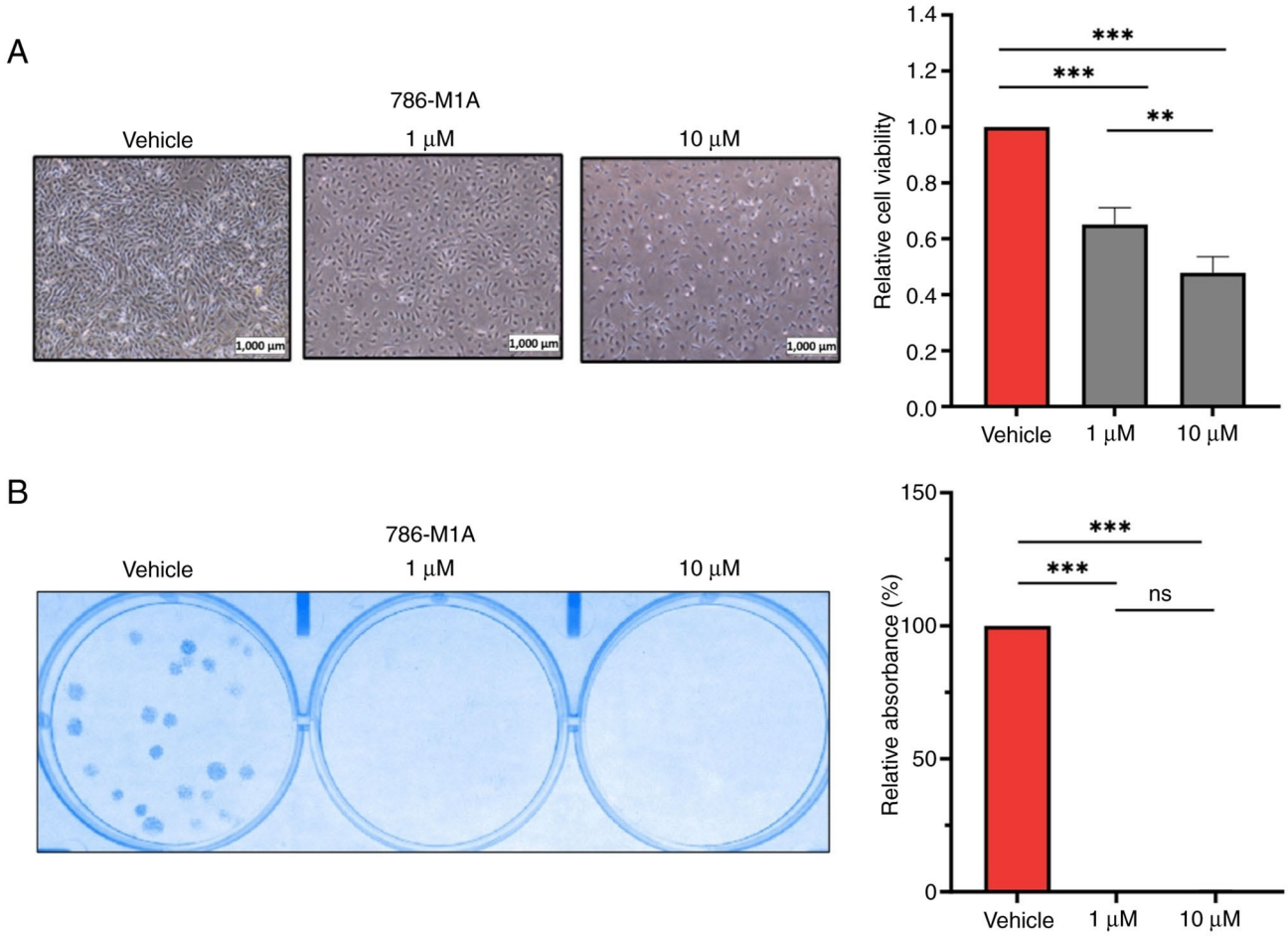

Figure 1. Bromodomain-containing 4 inhibition reduces ccRCC cell viability. Treatment with bromodomain-containing 4 inhibitor JQ1 reduced (A) viability and (B) colony formation in 786-M1A cells. P-values were determined by one-way ANOVA followed by Tukey's multiple-comparison post hoc test. **P<0.005, ***P<0.0005. ns, not significant.

inhibitors impairs *KLF6* transcriptional activation in ccRCC cells. For BRD4 inhibition, 786-M1A and OS-LM1B cells were treated with 1 or 10 μM JQ1 for 6 h, which was a time point shown to not affect cell viability (data not shown), followed by assessment of *KLF6* expression via qPCR analysis. Treatment with either 1 or 10 μM JQ1 significantly decreased *KLF6* expression in both ccRCC cell lines compared with vehicle-treated controls. Although *KLF6* downregulation was dose-dependent, the difference in the extent of reduction between 1 and 10 μM JQ1 was not significant (Fig. 3A).

To examine the role of p300, 786-M1A and OS-LM1B cells were treated with 1 or 10 μM A-485 for 16 h. qPCR analysis revealed that treatment with 1 μM A-485 did not significantly downregulate *KLF6* expression in either ccRCC cell line. However, treatment with the higher concentration of A-485 decreased *KLF6* expression by 50-60% in both 786-M1A and OS-LM1B cells (Fig. 3B). These findings underline the involvement of BRD4 and p300 in the regulation of *KLF6* expression in ccRCC.

H3K27ac signals are decreased following BRD4 and p300 inhibition. The present study investigated whether the downregulation of *KLF6* following BRD4 and p300 inhibition was associated with changes in the chromatin landscape at the *KLF6* SE region. H3K27ac ChIP-qPCR was performed to assess H3K27ac signal levels in JQ1- and A-485-treated 786-M1A cells. Constituent enhancers near the *KLF6* locus (SE_1, SE_2 and SE_3) were selected from our previous H3K27ac ChIP-Seq dataset in ccRCC (25) based on their enrichment signal and proximity to the *KLF6* promoter (Fig. 4A). Inhibition of BRD4 with 10 μM JQ1 decreased H3K27ac signals at all three constituent enhancers compared with those of vehicle-treated cells (Fig. 4B).

Similarly, treatment with the p300 inhibitor A-485 also decreased H3K27ac signals at these enhancer regions (Fig. 4C). As a negative control, IgG ChIP-qPCR was performed in parallel under the same conditions, which showed minimal background enrichment across all loci, confirming antibody specificity and negligible non-specific binding (Fig. 4B and C). Collectively, inhibition of BRD4 and p300 reduced H3K27ac signals, a marker of open chromatin and active transcription (7,10), at SE_1, SE_2 and SE_3 constituent enhancers, which potentially contributed to *KLF6* downregulation.

CRISPR-mediated deacetylation of SE_1 decreases KLF6 expression. A CRISPR-based approach was used to deacetylate the SE_1, SE_2 and SE_3 regions and assess the effects on chromatin accessibility and *KLF6* expression. Prior to generating the 786-M1A cells that stably express dCas9-HDAC3, the plasmid was modified to remove the stop codon between the

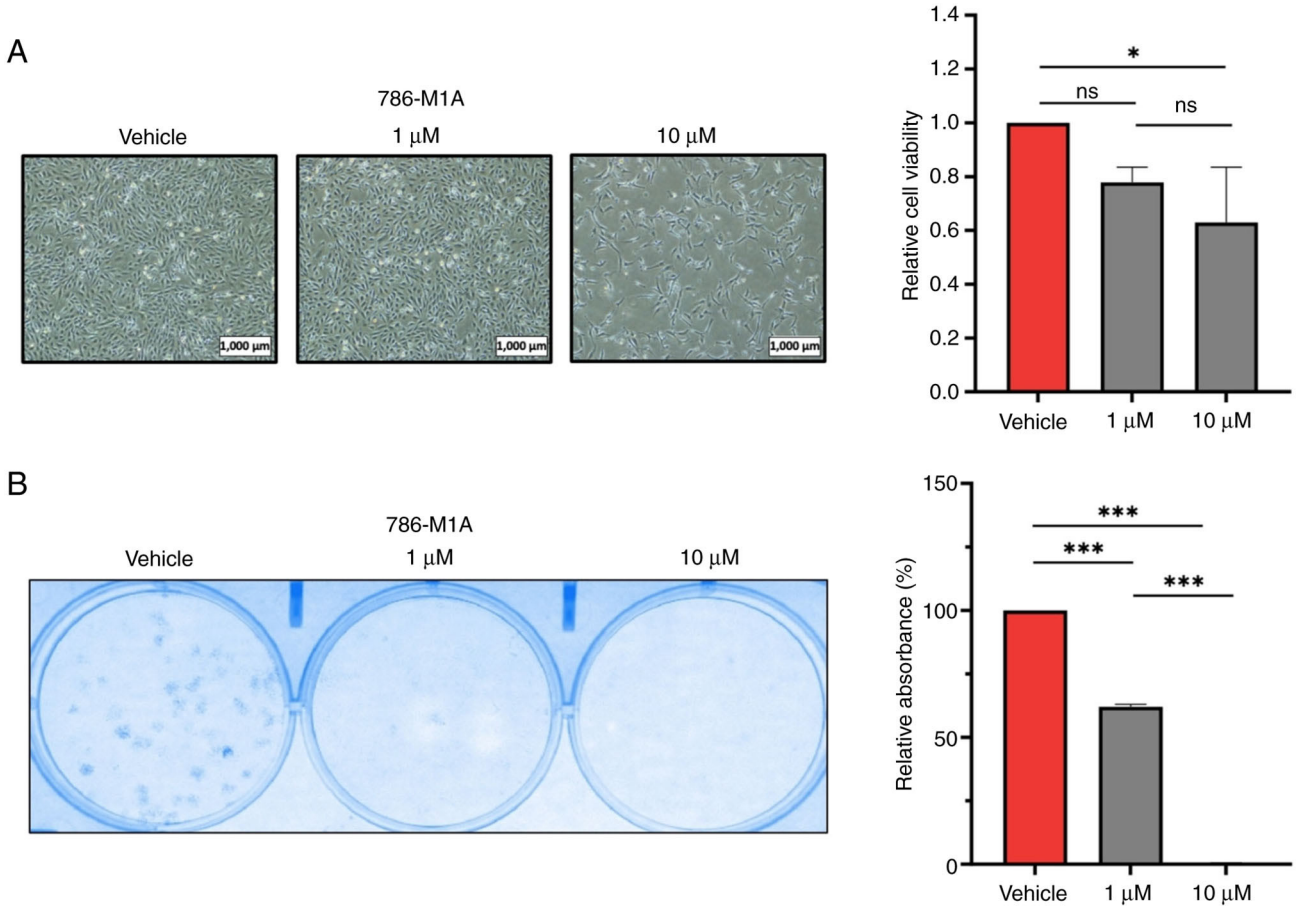

Figure 2. Inhibition of p300 suppresses ccRCC cell viability. Treatment with the p300 inhibitor A-485 reduced the (A) viability and (B) colony formation of 786-M1A cells. P-values were determined by one-way ANOVA followed by Tukey's multiple-comparison post hoc test. *P<0.05, ***P<0.0005. ns, not significant.

dCas9-HDAC3 and blasticidin-resistant gene reading frames (Fig. 5A). Site-directed mutagenesis was used to replace the stop codon (TAA) with alanine (AAA), allowing for blasticidin selection of cells that were successfully transduced with the dCas9-HDAC3-expressing plasmid (Fig. 5B and C). dCas9-HDAC3 protein expression in the transduced 786-M1A cells was confirmed by western blotting (Fig. 5D). These stable dCas9-HDAC3-expressing 786-M1A cells were transduced with either a non-targeting sgRNA control or iSE_1, iSE_2 and iSE_3 sgRNAs, which specifically target the SE_1, SE_2 or SE_3 enhancer regions, respectively. All sgRNAs were cloned into an sgRNA expression vector as described in our previous study (25). Western blot analysis confirmed stable expression of dCas9-HDAC3 in 786-M1A cells transduced with each sgRNA (Fig. 6A).

qPCR demonstrated ~25% *KLF6* expression downregulation in dCas9-HDAC3-expressing 786-M1A cells transduced with iSE_1 sgRNA. However, there was no significant decrease in *KLF6* expression in the iSE_2- and iSE_3-transduced cells (Fig. 6B). The downregulation of *KLF6* in the iSE_1-transduced cells suggested that the decreased *KLF6* expression may result from dCas9-HDAC3-mediated deacetylation of the SE_1 region. To assess the deacetylation efficiency, H3K27ac ChIP-qPCR was performed on the iSE_1 sgRNA-transduced cells. Decreased H3K27ac signals at the iSE_1-targeted enhancer indicated deacetylation of this region, which consequently altered chromatin accessibility and impaired *KLF6* transcription (Fig. 6C). As a negative control, parallel IgG ChIP-qPCR demonstrated low background signal at this locus, confirming the specificity of the antibody and minimal non-specific binding.

Discussion

The present findings revealed that BRD4 and p300, key epigenetic modifiers, serve integral roles in the regulation of chromatin accessibility within the *KLF6* SE region and drive high expression of this gene in ccRCC. These results align with previous research highlighting the key roles of BRD4 and p300 in sustaining SE activity and promoting the transcription of oncogenes in numerous types of cancer including breast and lung cancer and neuroblastoma (10,31,32). However, although inhibition of BRD4 or p300 significantly reduced *KLF6* expression in ccRCC cells, the magnitude of this reduction was moderate (40-50%). *KLF6* expression in ccRCC is driven by a large and robust SE region. Therefore, we hypothesized that redundancy mechanisms or the involvement of other epigenetic and transcriptional regulators may compensate for the loss of BRD4 or p300 activity, allowing the transcription of *KLF6* to persist despite inhibition of these SE regulators.

The modest downregulation of *KLF6* observed following JQ1 treatment may also reflect the intrinsic robustness of the large *KLF6* SE. Given its extensive size and modular architecture, partial inhibition of BRD4 may be insufficient to fully

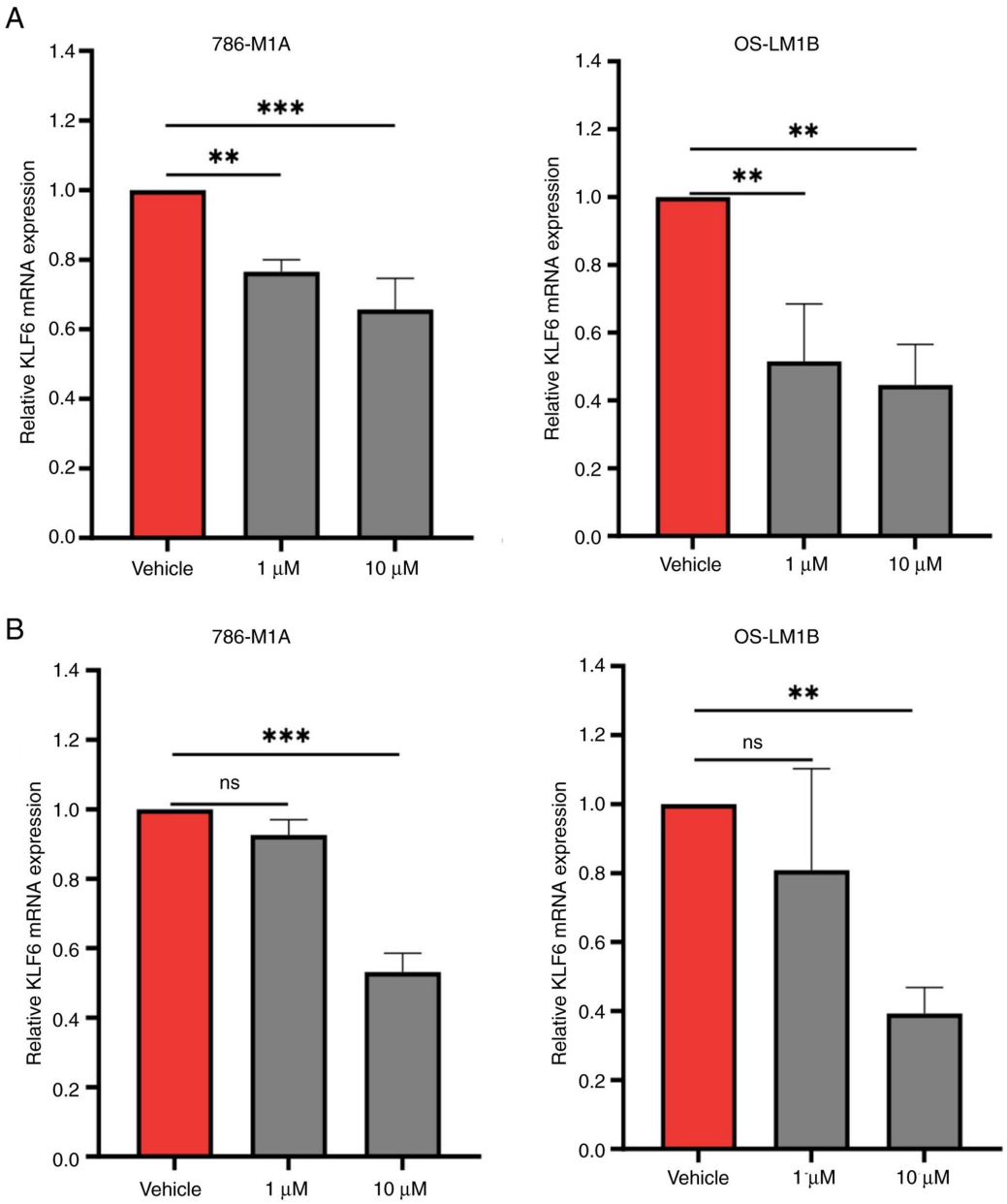

Figure 3. Bromodomain-containing 4 and p300 inhibition reduces *KLF6* expression. Pharmacological inhibition of (A) bromodomain-containing 4 using JQ1and (B) p300 using A-485 decreased *KLF6* expression in 786-M1A and OS-LM1B cells. P-values were determined by one-way ANOVA followed by Dunnett's multiple-comparison post hoc test. **P<0.005, ***P<0.0005. ns, not significant; KLF6, KLF transcription factor 6.

disrupt the transcriptional machinery assembled across all constituent enhancers (2). When BRD4 activity is decreased, residual occupancy of BRD4 or compensation by other bromodomain and extraterminal domain family members together with redundant enhancer modules within the SE may sustain sufficient chromatin accessibility and co-activator recruitment to maintain *KLF6* transcription (33). This is consistent with our previous study showing that simultaneous suppression of multiple constituent enhancers, or deletion of a large genomic region encompassing these multiple constituent enhancers, was required to achieve a more pronounced *KLF6* downregulation in ccRCC compared with individual enhancer perturbations (25). Additionally, it is possible that the JQ1 and A-485 treatment conditions did not result in complete inhibition of BRD4 and p300, respectively.

Our previous genome-wide H3K27ac ChIP-Seq profiling and CRISPR/Cas9 deletion of enhancer clusters upstream of *KLF6* provided direct evidence that this SE is functionally required for *KLF6* transcription in ccRCC (25). While genome-wide H3K27ac profiling was not performed in the present study, the targeted ChIP-qPCR and transcriptional assays in the present study focused specifically on previously validated SE constituents (25). The present study assessed H3K27ac signals in only three constituent enhancers via ChIP-qPCR. Although significant decreases in H3K27ac signals were observed at SE_1, SE_2 and SE_3 regions upon BRD4 and p300 inhibition, future studies should investigate the effect of these inhibitions on H3K27ac signals not only across the entire *KLF6* SE locus but also at the genome-wide level using ChIP-Seq. This comprehensive analysis may

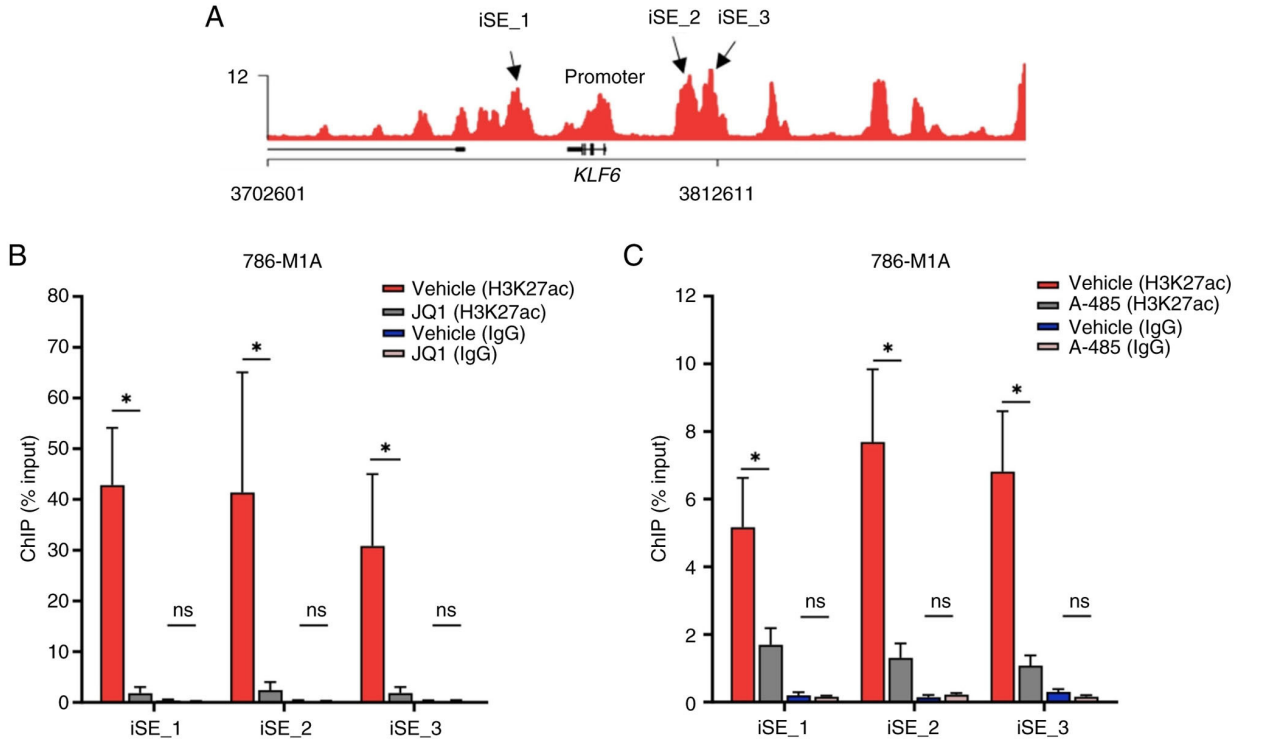

Figure 4. Changes in H3K27ac enrichment at the *KLF6* enhancer regions following BRD4 and p300 inhibition. (A) Schematic representation of three constituent enhancers located in proximity to the *KLF6* locus. (B) Pharmacological inhibition of BRD4 using JQ1 decreased the H3K27ac signal compared with the vehicle control. (C) Pharmacological inhibition of p300 using A-485 decreased the H3K27ac signal compared with the vehicle control. IgG ChIP-quantitative PCR showed minimal enrichment at all *KLF6* enhancer regions following treatment with JQ1 and A-485, as well as their respective vehicle controls, confirming low background signal. P-values were determined using unpaired t-test with Welch's correction. *P<0.05. ns, not significant; H3K27ac, acetylation at lysine 27 of histone H3; KLF6, Kruppel-like factor 6; BRD4, bromodomain-containing 4; iSE, Clustered Regularly Interspaced Short Palindromic Repeats Interference-targeted super enhancer; ChIP, chromatin immunoprecipitation.

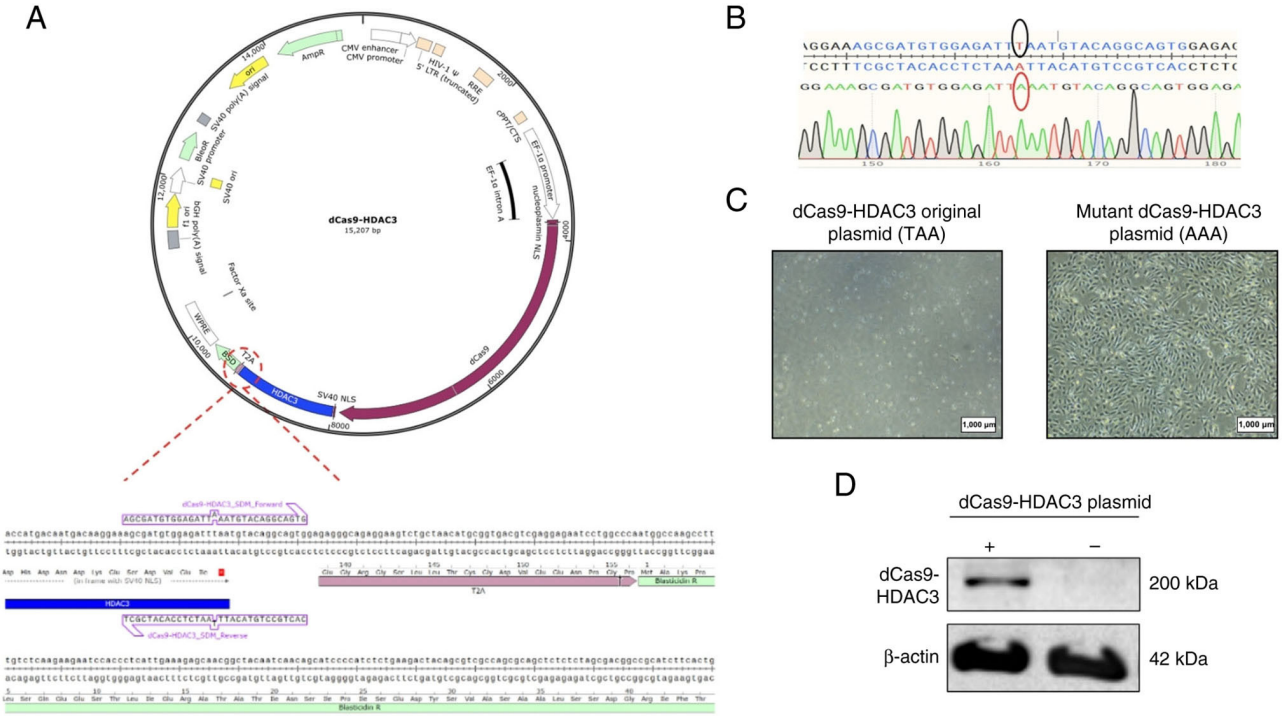

Figure 5. Validation of stop codon (TAA) removal in the original dCas9-HDAC3 plasmid. (A) Schematic representation of the stop codon located between the dCas9-HDAC3 coding sequence and blasticidin resistance gene fragments. The binding sites of the site-directed mutagenesis forward and reverse primers used to replace the stop codon with an alanine codon (AAA) are shown. (B) Electropherogram showing the successful nucleotide substitution from T to A. (C) Clear cell renal cell carcinoma cells transduced with the mutant dCas9-HDAC3 plasmid survived blasticidin selection, confirming successful removal of the stop codon. (D) Western blot analysis confirmed dCas9-HDAC3 expression in 786-M1A cells transduced with the dCas9-HDAC3 plasmid (+) compared with non-transduced cells (-). dCas9-HDAC3, dead Cas9-histone deacetylase 3.

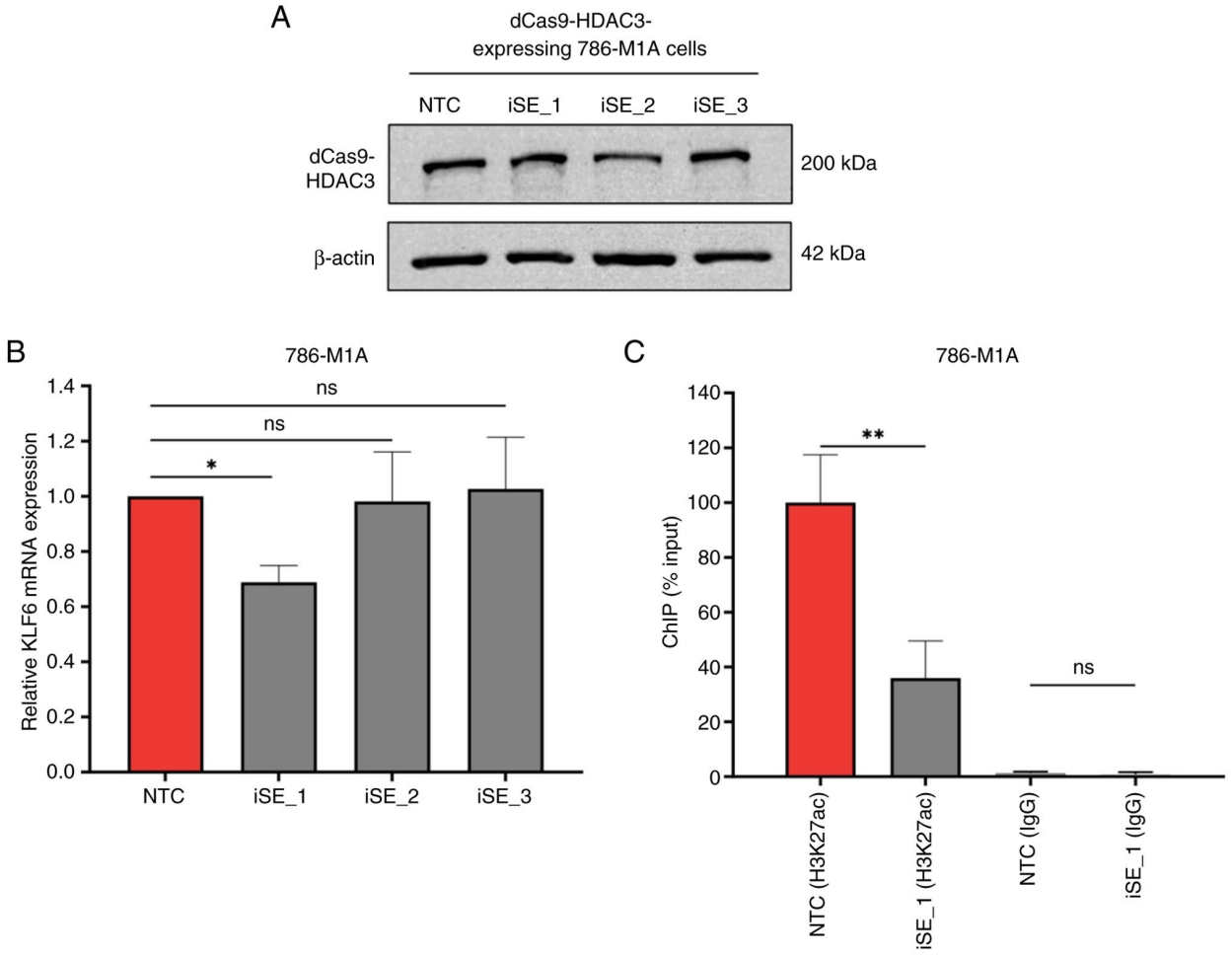

Figure 6. CRISPR-mediated deacetylation of SE_1 decreases *KLF6* expression. (A) Western blot analysis confirmed stable dCas9-HDAC3 expression in 786-M1A cells transduced with single guide RNAs. (B) qPCR analysis showed reduced *KLF6* expression in iSE_1-transduced cells compared with NTC cells. P-values were determined by one-way ANOVA followed by Dunnett's multiple-comparison post hoc test. (C) ChIP-qPCR showed decreased H3K27ac enrichment at SE_1 in iSE_1-transduced cells compared with NTC cells. IgG ChIP-qPCR showed minimal enrichment at SE_1 in both NTC and iSE_1 transduced cells, confirming low background signal and antibody specificity. P-values were determined using an unpaired t-test with Welch's correction. *P<0.05, **P<0.005. dCas9-HDAC3, dead Cas9-histone deacetylase 3; qPCR, quantitative PCR; KLF6, Kruppel-like factor 6; iSE, CRISPRi-targeted super enhancer; NTC, non-targeting control; ChIP, chromatin immunoprecipitation; H3K27ac, acetylation at lysine 27 of histone H3; ns, not significant.

allow for a deeper understanding of the global chromatin modifications induced by these inhibitors and their broader impact on gene expression regulation.

The present study deepens understanding of the KLF6 transcriptional networks in ccRCC by elucidating the roles of the epigenetic regulators BRD4 and p300 in governing this process. These insights may pave the way for the development of novel diagnostic and therapeutic strategies for ccRCC. Although inhibition of BRD4 and p300 decreased H3K27ac signals and *KLF6* expression, it remains uncertain whether the decreased viability in BRD4- or p300-inhibited cells is directly linked to perturbation in the KLF6 transcriptional network. As BRD4 and p300 are essential epigenetic and transcriptional regulators, targeting these proteins affects genome-wide transcriptional activity, suggesting that the phenotypic impacts of these inhibitors may extend beyond the direct regulation of *KLF6* expression. As shown in our previous study, *KLF6* knockdown impairs ccRCC cell proliferation and decreases *PDGFβ* transcription, supporting its key role in cell viability and downstream signaling (25). These data support KLF6 as a key effector of BRD4/p300-regulated phenotypes. In line with this, BRD4 inhibition suppresses ccRCC cell proliferation and epithelial-to-mesenchymal transition by activating the NF-κB/NLR family pyrin domain containing 3/caspase-1 pyroptosis signaling pathway (34). JQ1-mediated BRD4 inhibition exerts anticancer effects in ccRCC by downregulating the expression of numerous oncogenes, including *MYC* (35). On the other hand, Dong *et al* (36) used a computational approach to link normal developmental programs to cancer-specific driver mutations. The aforementioned study identified a regulatory network associated with a poor prognosis subtype, classified as the C0 group, that was maintained by p300. Analysis of drug response data from ccRCC cell lines predicted to be in the C0 group revealed that 8 out of 15 cell lines were sensitive to the p300 inhibitor A-485 (36).

Although several studies, including the present study, have demonstrated the inhibitory effects of JQ1 and A-485 on ccRCC cell viability (34-37), their impact on normal cells and potential genome-wide consequences warrant further investigation. A challenge in targeting SEs for cancer treatment is specificity. This is because the main SEs and transcription regulatory proteins such as BRD4 and p300 also serve key roles

in modulating normal cell and physiological processes (1,2), making it difficult to selectively target cancer cells without affecting normal cell function. Therefore, it is crucial to determine the SE-driven transcriptional networks that are governed by these epigenetic regulators. By identifying other candidate proteins or pathways that are specifically active in cancer cells, it may be possible to develop more targeted therapies with minimal off-target effects on normal cells. For example, our previous study identified a cell signaling loop that links SE-driven KLF6 to mTORC1 signaling hyperactivation and lipid metabolism, which support ccRCC cell proliferation and progression (25). KLF6 serves a central role in regulating this cellular network by transactivating the expression of pro-angiogenic *PDGFβ*, a key agonist of the mTORC1 signaling pathway (25,38). The upregulation of angiogenesis and hyperactivation of the mTORC1 signaling pathway are ccRCC hallmark features; a number of clinically approved therapies for ccRCC have been designed to target these phenotypes, including the angiogenesis inhibitors sunitinib and axitinib as well as the mTORC1 pathway inhibitors everolimus and temsirolimus (39). Collectively, the aforementioned findings on KLF6 underscore the importance of a comprehensive investigation and understanding of SE regulation and activity, as well as downstream cellular networks, to uncover cancer-specific drivers and identify novel therapeutic targets.

Advancements in CRISPR technology have led to the evolution of its applications beyond traditional gene editing. The present study used the CRISPR-mediated histone deacetylation tool to assess its efficiency in perturbing *KLF6* SE activity and the transcription of this gene. Of the three constituent enhancers, modest downregulation of *KLF6* expression was observed only in SE_1-targeted cells. This corroborates our previous study on the robustness of this SE region and its modular function in driving *KLF6* expression in ccRCC (25). In our previous study, a marked reduction in *KLF6* expression was only achieved when multiple constituent enhancers were concurrently suppressed using CRISPRi or by deleting large genomic region containing these multiple clusters of enhancer using traditional CRISPR/Cas9 (25). These findings contrast with numerous studies that have shown that cancer-associated SEs are sensitive to perturbations of constituent enhancers or the components responsible for regulating the SE landscape (38-40). Nonetheless, the redundancy and robustness in the regulation of *KLF6* SE activity and transcription are aligned with the role of KLF6 in driving ccRCC phenotypes (25). Most key biological processes and developmental transcriptional programs are relatively insensitive to genetic changes or environmental perturbations, reflecting regulatory robustness (42).

The HDAC family comprises >10 members, including HDAC3 (43). Given the diverse regulatory functions and substrates of HDACs (43), dCas9-HDAC3 alone may not be sufficient to efficiently deacetylate the targeted constituent enhancers. A more comprehensive approach, potentially involving deacetylation by multiple HDACs, warrants further investigation to evaluate the efficiency of the CRISPR approach in modifying the chromatin landscape and modulating transcriptional regulation. Future studies should evaluate dCas9 fusions with alternative HDAC isoforms to determine whether specific HDACs display higher efficiency at renal SE regions.

A limitation of this study is the absence of non-tumorigenic renal epithelial as well as non-renal cancer models, precluding definitive assessment of whether BRD4/p300-dependent *KLF6* super-enhancer regulation is ccRCC-specific. Future studies including such models will be necessary to establish lineage specificity. This is particularly relevant because renal enhancer identity and transcriptional programs in ccRCC are shaped by renal lineage factors such as paired box 8 (44). JQ1 and A-485 exert broad epigenetic effects and *KLF6* downregulation may not be exclusively due to direct SE disruption. However, our previous study demonstrated that genetic perturbation of *KLF6* or its upstream enhancer cluster result in similar phenotypes, including suppression of mTORC1-associated signaling and decreased ccRCC cell viability (20). While the present study did not perform *KLF6* rescue experiments following BRD4 or p300 inhibition, the consistent decrease in *KLF6* expression and associated phenotypes support its functional contribution. Future studies incorporating *KLF6* rescue or epistasis analyses following pharmacological perturbation would be valuable to further clarify this causal association. Additionally, genome-wide approaches such as RNA-sequencing and H3K27ac ChIP-seq following BRD4 or p300 inhibition would help distinguish KLF6-dependent effects from broader transcriptional and chromatin changes.

In conclusion, the present study revealed that BRD4 and p300 are key regulators of *KLF6* super-enhancer activity in ccRCC. Together with our previous findings demonstrating the super enhancer activity in driving high *KLF6* expression (25), these results further highlight BRD4 and p300 as potential therapeutic targets in this cancer. Additionally, targeted deacetylation of *KLF6* enhancer regions using dCas9-HDAC3 demonstrated that deacetylation of an individual region was insufficient to fully suppress *KLF6* expression. This observation aligns with our previous study, which highlighted the robustness of the *KLF6* SE and the existence of regulatory redundancy or compensatory mechanisms within this SE landscape (25). Future research employing combinatorial epigenetic perturbation strategies may provide valuable insights into the complex regulatory networks of SEs in cancer, potentially leading to the development of more effective and targeted therapeutic approaches.

Acknowledgements

The authors would like to thank Professor Dr Joan Massagué, Memorial Sloan Kettering Cancer Center, NY, USA, for providing the 786-M1A and OS-LM1B ccRCC cell lines. We also thank Dr Marston Linehan, National Cancer Institute, MD, USA, for providing the UOK101 ccRCC cell line.

Funding

The present study was supported by Geran Universiti Penyelidikan, Universiti Kebangsaan Malaysia (grant no. GUP-2023-005), the Dr Ranjeet Bhagwan Singh Medical Research Grant (grant no. JJ-2020-005) and the Ministry of Higher Education Fundamental Research Grant Scheme (grant no. FRGS/1/2020/SKK0/UKM/03/3).

Availability of data and materials

The data generated in the present study may be requested from the corresponding author.

Authors' contributions

SES and MAM conceived and designed the study and edited the manuscript. SES, NNMZ, AYA, NQAAR and SNHMY performed experiments. SES and NNMZ analyzed the data and wrote the manuscript. SES, NNMZ and NQAAR confirm the authenticity of all the raw data. All authors have read and approved the final version of the manuscript.

Ethics approval and consent to participate

Not applicable.

Patient consent for publication

Not applicable.

Competing interests

The authors declare that they have no competing interests.

References

1. Whyte WA, Orlando DA, Hnisz D, Abraham BJ, Lin CY, Kagey MH, Rahl PB, Lee TI and Young RA: Master transcription factors and mediator establish super-enhancers at key cell identity genes. Cell 153: 307-319, 2013.
2. Hnisz D, Abraham BJ, Lee TI, Lau A, Saint-André V, Sigova AA, Hoke HA and Young RA: Super-enhancers in the control of cell identity and disease. Cell 155: 934-947, 2013.
3. Zhou RW and Parsons RE: Etiology of super-enhancer reprogramming and activation in cancer. Epigenetics Chromatin 16: 29, 2023.
4. Sengupta S and George RE: Super-enhancer-driven transcriptional dependencies in cancer. Trends Cancer 3: 269-281, 2017.
5. Tang F, Yang Z, Tan Y and Li Y: Super-enhancer function and its application in cancer targeted therapy. NPJ Precis Oncol 4: 2, 2020.
6. Filippakopoulos P, Qi J, Picaud S, Shen Y, Smith WB, Fedorov O, Morse EM, Keates T, Hickman TT, Felletar I, *et al*: Selective inhibition of BET bromodomains. Nature 468: 1067-1073, 2010.
7. Chiang CM: Brd4 engagement from chromatin targeting to transcriptional regulation: selective contact with acetylated histone H3 and H4. F1000 Biol Rep 1: 98, 2009.
8. Qian H, Zhu M, Tan X, Zhang Y, Liu X and Yang L: Super-enhancers and the super-enhancer reader BRD4: tumorigenic factors and therapeutic targets. Cell Death Discov 9: 1-11, 2023.
9. Donati B, Lorenzini E and Ciarrocchi A: BRD4 and cancer: Going beyond transcriptional regulation. Mol Cancer 17: 164, 2018.
10. Wang M, Chen Q, Wang S, Xie H, Liu J, Huang R, Xiang Y, Jiang Y, Tian D and Bian E: Super-enhancers complexes zoom in transcription in cancer. J Exp Clin Cancer Res 42: 183, 2023.
11. Strachowska M and Robaszkiewicz A: Characteristics of anticancer activity of CBP/p300 inhibitors-Features of their classes, intracellular targets and future perspectives of their application in cancer treatment. Pharmacol Ther 257: 108636, 2024.
12. Chen Q, Yang B, Liu X, Zhang XD, Zhang L and Liu T: Histone acetyltransferases CBP/p300 in tumorigenesis and CBP/p300 inhibitors as promising novel anticancer agents. Theranostics 12: 4935-4948, 2022.
13. Adli M: The CRISPR tool kit for genome editing and beyond. Nat Commun 9: 1911, 2018.
14. Zamberi NN, Abuhamad AY, Low TY, Mohtar MA and Syafruddin SE: dCas9 tells tales: Probing gene function and transcription regulation in cancer. CRISPR J 7: 73-87, 2024.
15. Wang Q, Ma C, Mao H and Wang J: Epigenome editing by a CRISPR-Cas9-based acetyltransferase activates the ZNF334 gene to inhibit the growth of colorectal cancer. Int J Biol Macromol 277: 134580, 2024.
16. Wang L, Wang E, Balcazar JP, Wu Z, Xiang K, Wang Y, Huang Q, Negrete M, Chen KY, Li W, *et al*: Chromatin remodeling of colorectal cancer liver metastasis is mediated by an HGF-PU.1-DPP4 axis. Adv Sci (Weinh) 8: e2004673, 2021.
17. Liu J, Sun M, Cho KB, Gao X and Guo B: A CRISPR-Cas9 repressor for epigenetic silencing of KRAS. Pharmacol Res 164: 105304, 2021.
18. Hsieh JJ, Purdue MP, Signoretti S, Swanton C, Albiges L, Schmidinger M, Heng DY, Larkin J and Ficarra V: Renal cell carcinoma. Nat Rev Dis Primers 3: 17009, 2017.
19. Barragan-Carrillo R, Saad E, Saliby RM, Sun M, Albiges L, Bex A, Heng D, Mejean A, Motzer RJ, Plimack ER, *et al*: First and second-line treatments in metastatic renal cell carcinoma. Eur Urol 87: 143-154, 2025.
20. Mattila KE, Vainio P and Jaakkola PM: Prognostic factors for localized clear cell renal cell carcinoma and their application in adjuvant therapy. Cancers (Basel) 14: 239, 2022.
21. Turajlic S, Xu H, Litchfield K, Rowan A, Horswell S, Chambers T, O'Brien T, Lopez JI, Watkins TBK, Nicol D, *et al*: Deterministic evolutionary trajectories influence primary tumor growth: TRACERx renal. Cell 173: 595-610, 2018.
22. Aweys H, Lewis D, Sheriff M, Rabbani RD, Lapitan P, Sanchez E, Papadopoulos V, Ghose A and Boussios S: Renal cell cancer-insights in drug resistance mechanisms. Anticancer Res 43: 4781-4792, 2023.
23. Makhov P, Joshi S, Ghatalia P, Kutikov A, Uzzo RG and Kolenko VM: Resistance to systemic therapies in clear cell renal cell carcinoma: mechanisms and management strategies. Mol Cancer Ther 17: 1355-1364, 2018.
24. Lovén J, Hoke HA, Lin CY, Lau A, Orlando DA, Vakoc CR, Bradner JE, Lee TI and Young RA: Selective inhibition of tumor oncogenes by disruption of super-enhancers. Cell 153: 320-334, 2013.
25. Syafruddin SE, Rodrigues P, Vojtasova E, Patel SA, Zaini MN, Burge J, Warren AY, Stewart GD, Eisen T, Bihary D, *et al*: A KLF6-driven transcriptional network links lipid homeostasis and tumour growth in renal carcinoma. Nat Commun 10: 1-13, 2019.
26. Vanharanta S, Shu W, Brenet F, Hakimi AA, Heguy A, Viale A, Reuter VE, Hsieh JJ, Scandura JM and Massagué J: Epigenetic expansion of VHL-HIF signal output drives multiorgan metastasis in renal cancer. Nat Med 19: 50-56, 2013.
27. Kwon DY, Zhao YT, Lamonica JM and Zhou Z: Locus-specific histone deacetylation using a synthetic CRISPR-Cas9-based HDAC. Nat Commun 8: 15315, 2017.
28. Schmittgen TD and Livak KJ: Analyzing real-time PCR data by the comparative CT method. Nat Protoc 3: 1101-1108, 2008.
29. Qi LS, Larson MH, Gilbert LA, Doudna JA, Weissman JS, Arkin AP and Lim WA: Repurposing CRISPR as an RNA-guided platform for sequence-specific control of gene expression. Cell 152: 1173-1183, 2013.
30. Haring M, Offermann S, Danker T, Horst I, Peterhansel C and Stam M: Chromatin immunoprecipitation: Optimization, quantitative analysis and data normalization. Plant Methods 3: 11, 2007.
31. Jia Q, Chen S, Tan Y, Li Y and Tang F: Oncogenic super-enhancer formation in tumorigenesis and its molecular mechanisms. Exp Mol Med 52: 713-723, 2020.
32. Thandapani P: Super-enhancers in cancer. Pharmacol Ther 199: 129-138, 2019.
33. Sarnik J, Popławski T and Tokarz P: BET proteins as attractive targets for cancer therapeutics. Int J Mol Sci 22: 11102, 2021.
34. Tan YF, Wang M, Chen ZY, Wang L and Liu XH: Inhibition of BRD4 prevents proliferation and epithelial-mesenchymal transition in renal cell carcinoma via NLRP3 inflammasome-induced pyroptosis. Cell Death Dis 11: 239, 2020.
35. Sakaguchi T, Yoshino H, Sugita S, Miyamoto K, Yonemori M, Osako Y, Meguro-Horike M, Horike SI, Nakagawa M and Enokida H: Bromodomain protein BRD4 inhibitor JQ1 regulates potential prognostic molecules in advanced renal cell carcinoma. Oncotarget 9: 23003-23017, 2018.
36. Dong X, Zhang D, Zhang X, Liu Y and Liu Y: Network modeling links kidney developmental programs and the cancer type-specificity of VHL mutations. NPJ Syst Biol Appl 10: 114, 2024.
37. Kuang Z, Guo K, Cao Y, Jiang M, Wang C, Wu Q, Hu G, Ao M, Huang M, Qin J, *et al*: The novel CDK9 inhibitor, XPW1, alone and in combination with BRD4 inhibitor JQ1, for the treatment of clear cell renal cell carcinoma. Br J Cancer 129: 1915-1929, 2023.

38. Abuhamad AY, Zamberi NN, Vanharanta S, Yusuf SNH, Mohtar MA and Syafruddin SE: Cancer cell-derived PDGFB stimulates mTORC1 activation in renal carcinoma. Int J Mol Sci 24: 6447, 2023.
39. Choueiri TK and Motzer RJ: Systemic therapy for metastatic renal-cell carcinoma. N Engl J Med 376: 354-366, 2017.
40. Chipumuro E, Marco E, Christensen CL, Kwiatkowski N, Zhang T, Hatheway CM, Abraham BJ, Sharma B, Yeung C, Altabef A, *et al*: CDK7 inhibition suppresses super-enhancer-linked oncogenic transcription in MYCN-driven cancer. Cell 159: 1126-1139, 2014.
41. Bhagwat AS, Roe J-S, Mok BYL, Hohmann AF, Shi J and Vakoc CR: BET bromodomain inhibition releases the mediator complex from select cis-regulatory elements. Cell Rep 15: 519-530, 2016.
42. Félix MA and Barkoulas M: Pervasive robustness in biological systems. Nat Rev Genet 16: 483-496, 2015.
43. Seto E and Yoshida M: Erasers of histone acetylation: The histone deacetylase enzymes. Cold Spring Harb Perspect Biol 6: a018713, 2014.
44. Patel SA, Hirosue S, Rodrigues P, Vojtasova E, Richardson EK, Ge J, Syafruddin SE, Speed A, Papachristou EK, Baker D, *et al*: The renal lineage factor PAX8 controls oncogenic signalling in kidney cancer. Nature 606: 999-1006, 2022.